Signal Drop in Mass Density Profiles: Combining Lensing Simulations and Observations

David Crespo

(Joaquin Gonzalez-Nuevo, Laura Bonavera, Marcos M. Cueli, Rebeca Fernández-Fernández & Jose Manuel Casas)

Oviedo; June 20, 2025

[Crespo et al. 2024; Crespo et al. 2025 (submitted)]

ICTEA Instituto Universitario de Ciencias y Tecnologías Espaciales de Asturias

Jornadas del ICTEA 2025
ICTEA Days 2025

Universidad de Oviedo

Magnification bias

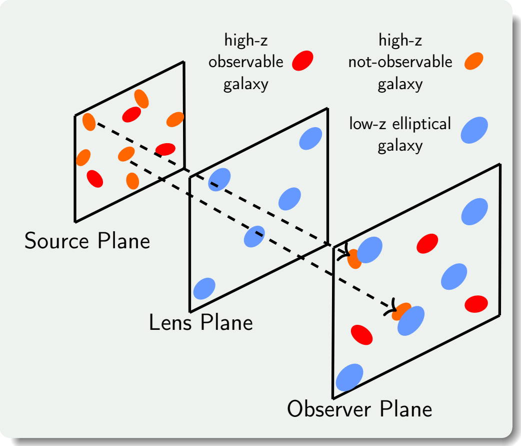

. . . is a gravitational lensing effect.
Excess/Deficit of background sources nearby the lens position

Magnification bias

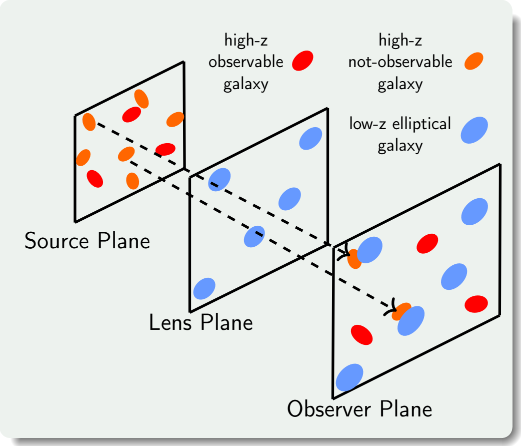

. . . is a gravitational lensing effect. Excess/Deficit of background sources nearby the lens position

$$N(>S) = N_0 S^{-\beta}$$

$\beta > 1 \rightarrow$ Amplification

$\beta > 2 \rightarrow$ Optimal for Weak lensing events

Magnification bias

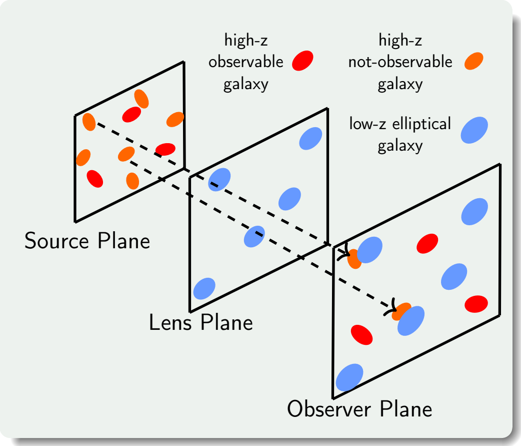

...is a gravitational lensing effect. Excess/Deficit of background sources nearby the lens position

$$N(>S) = N_0 S^{-\beta}$$

$\beta > 1 \rightarrow$ Amplification

$\beta > 2 \rightarrow$ Optimal for Weak lensing events

direct probe of total mass ($\sim$ dark matter)

Magnification bias

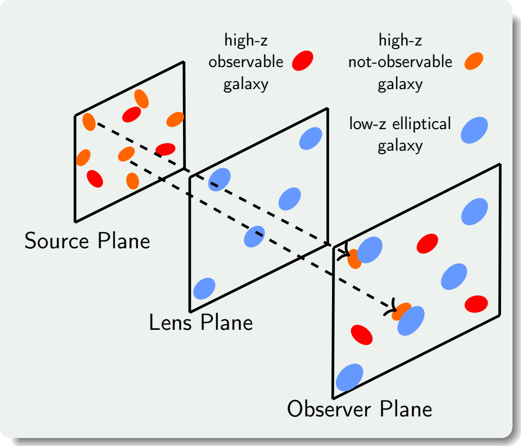

. . . is a gravitational lensing effect. Excess/Deficit of background sources nearby the lens position

$$N(>S) = N_0 S^{-\beta}$$

$\beta > 1 \rightarrow$ Amplification

$\beta > 2 \rightarrow$ Optimal for Weak lensing events

direct probe of total mass ($\sim$ dark matter)

. . . foreground-background number correlation

1 Introduction

2 Data and Methodology

3 Results

4 Conclusions

The background and foreground samples

Background sample: **Sub-millimetre galaxies** (SMGs) by Herschel Space Observatory in H-ATLAS (e.g. Eales et al. 2010, Valiante et al. 2016)

The background and foreground samples

Background sample: **Sub-millimetre galaxies** (SMGs) by Herschel Space Observatory in H-ATLAS (e.g. Eales et al. 2010, Valiante et al. 2016)

1. High redshift distribution
2. Steep source number counts
3. Fairly invisible in the optical band

The background and foreground samples

Background sample: **Sub-millimetre galaxies** (SMGs) by Herschel Space Observatory in H-ATLAS (e.g. Eales et al. 2010, Valiante et al. 2016)

1. High redshift distribution
2. Steep source number counts
3. Fairly invisible in the optical band

The background and foreground samples

Background sample: **Sub-millimetre galaxies** (SMGs) by Herschel Space Observatory in H-ATLAS (e.g. Eales et al. 2010, Valiante et al. 2016)

1. High redshift distribution
2. Steep source number counts
3. Fairly invisible in the optical band

The background and foreground samples

Background sample: **Sub-millimetre galaxies** (SMGs) by Herschel Space Observatory in H-ATLAS (e.g. Eales et al. 2010, Valiante et al. 2016)

1. High redshift distribution
2. Steep source number counts
3. Fairly invisible in the optical band

Optimal background sources for weak lensing studies!

The background and foreground samples

Background sample: **Sub-millimetre galaxies** (SMGs) by Herschel Space Observatory in H-ATLAS (e.g. Eales et al. 2010, Valiante et al. 2016)

1. High redshift distribution
2. Steep source number counts
3. Fairly invisible in the optical band

Optimal background sources for weak lensing studies!

Improve positional accuracy: **SMGs** by a cross match with NASA's Wide-field Infrared (WISE, Wright et al. 2010) and H-ATLAS

The background and foreground samples

Foreground samples:

- **Galaxies** in the GAMA II spectroscopic survey (Driver et al. 2011; Baldry et al. 2010, 2014; Liske et al. 2015)

  Overlapping: GAMA(9h,12h,14.5h) region

- **Quasi-stellar Objects** (QSOs) in SDSS-II and SDSS-III; DR7(Schneider et al. 2010) and DR12 (Pâris et al. 2017)

  Overlapping: GAMA(9h,12h,14.5h) and NGP regions

- **Clusters** by Sloan Digital Sky Survey III (SDSS III) (Wen et al. 2012)

  Overlapping: GAMA(9h,12h,14.5h) and NGP regions

- **Clusters** by SDSS (Zou et al. 2021)

  Overlapping: GAMA(9h,12h,14.5h) and NGP regions

The background and foreground samples

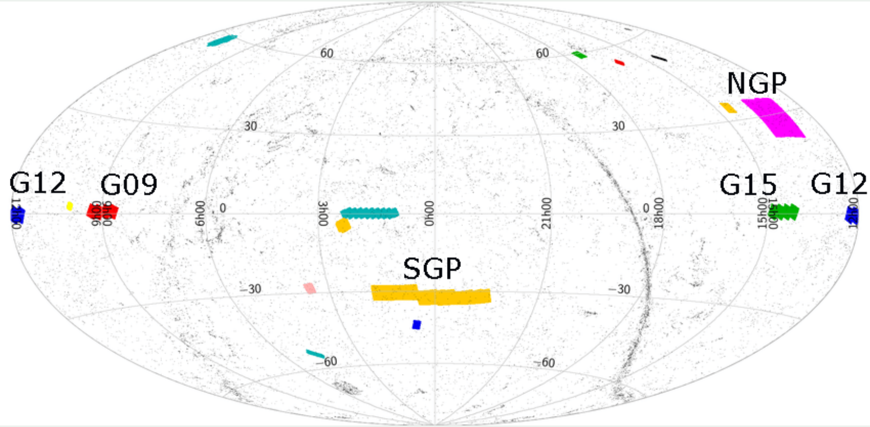

J. Greenslade et al. 2017

The background and foreground samples

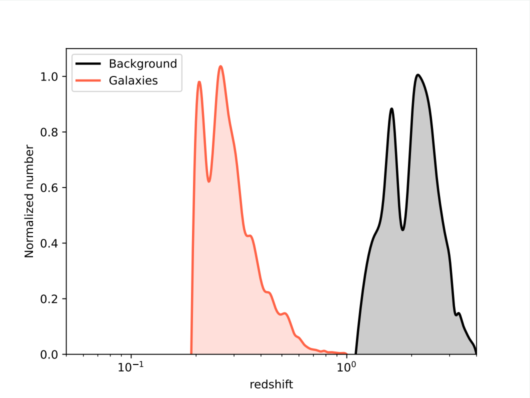

Background (SMGs):

(32.306) (64065)

$1.2 < z_{phot} < 4.0$

Foreground:

- Galaxies (102.672)
  $0.2 < z_{spec} < 1.0$
- QSOs (1.546)
  $0.2 < z_{spec} < 1.0$
- Clusters (3.651)
  $0.05 < z_{spec} < 0.8$
- Clusters ZOU (9.056)
  $0.05 < z_{spec} < 0.8$

The background and foreground samples

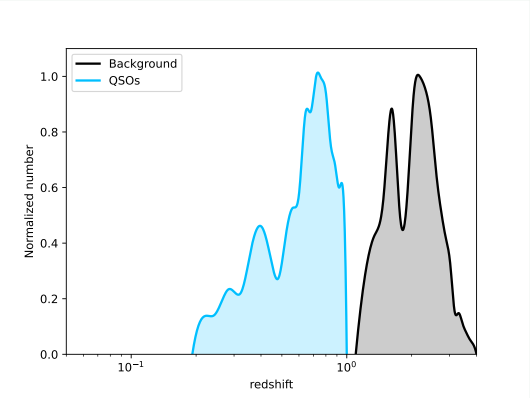

Background (SMGs):

(32.306) (64065)

$1.2 < z_{phot} < 4.0$

Foreground:

- Galaxies (102.672)
  $0.2 < z_{spec} < 1.0$
- QSOs (1.546)
  $0.2 < z_{spec} < 1.0$
- Clusters (3.651)
  $0.05 < z_{spec} < 0.8$
- Clusters ZOU (9.056)
  $0.05 < z_{spec} < 0.8$

The background and foreground samples

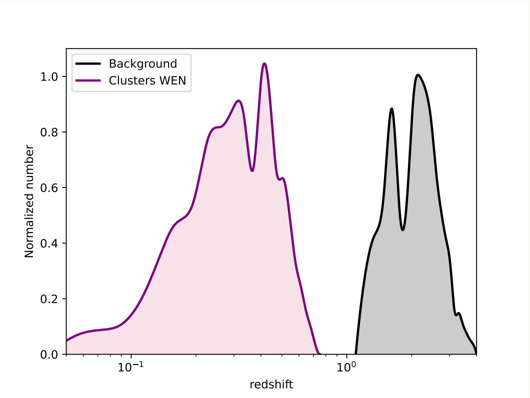

Background (SMGs):

(32.306) (64065)

$1.2 < z_{phot} < 4.0$

Foreground:

- Galaxies (102.672)
  $0.2 < z_{spec} < 1.0$
- QSOs (1.546)
  $0.2 < z_{spec} < 1.0$
- Clusters WEN (3.651)
  $0.05 < z_{spec} < 0.8$
- Clusters ZOU (9.056)
  $0.05 < z_{spec} < 0.8$

The background and foreground samples

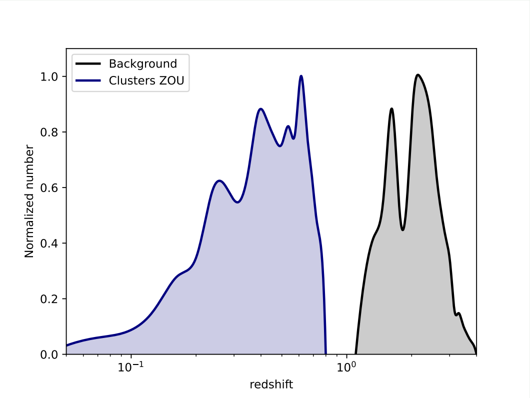

Background (SMGs):

(32.306) (64065)

$1.2 < z_{phot} < 4.0$

Foreground:

- Galaxies (102.672)
  $0.2 < z_{spec} < 1.0$
- QSOs (1.546)
  $0.2 < z_{spec} < 1.0$
- Clusters (3.651)
  $0.05 < z_{spec} < 0.8$
- Clusters ZOU (9.056)
  $0.05 < z_{spec} < 0.8$

Stacking

Advantages:

1. Positional errors
2. Follow the pairs contributing to the final stacked map

Stacking

Advantages:

1. Positional errors
2. Follow the pairs contributing to the final stacked map

Search radius $\begin{cases} 100 arcsec \longrightarrow 400\text{x}400\text{pixels} \\ 50\ arcsec \longrightarrow 2000\text{x}2000\text{pixels} \end{cases} \longrightarrow$ Data Stacking Map [DD]

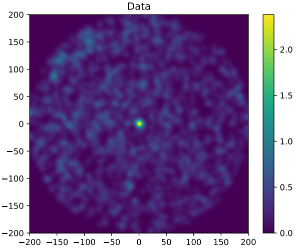

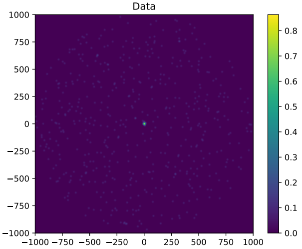

Stacking

Advantages:

1. Positional errors
2. Follow the pairs contributing to the final stacked map

$$\text{Search radius}\begin{cases} 100\,arcsec \longrightarrow \text{400x400pixels} \\ 50\ arcsec \longrightarrow \text{2000x2000pixels} \end{cases} \longrightarrow \text{Data Stacking Map [DD]}$$

We compute the RR term theoretically from the annulus area considering a constant surface density

Stacking

Advantages:

1. Positional errors
2. Follow the pairs contributing to the final stacked map

$$\text{Search radius}\begin{cases} 100arcsec \longrightarrow 400\text{x}400\text{pixels} \\ 50\ arcsec \longrightarrow 2000\text{x}2000\text{pixels} \end{cases} \longrightarrow \text{Data Stacking Map [DD]}$$

We compute the RR term theoretically from the annulus area considering a constant surface density

The CCF estimator (Davis & Peebles et al. ,1983):

$$\tilde{w}_x(\theta) = \frac{\text{DD}}{\text{RR}} - 1$$

Mass density profiles

CCF between lenses-background

$$w_x(\theta; z_l, z_b) = \mu^{\beta-1} - 1$$

Mass density profiles

CCF between lenses-background

$$w_x(\theta; z_l, z_b) = \mu^{\beta-1} - 1$$

Navarro-Frenk-White profile (NFW)

$$\rho_{NFW} = \frac{\rho_s}{(r/r_s)(1 + r/r_s)^2}$$

Mass density profiles

CCF between lenses-background

$$w_x(\theta; z_l, z_b) = \mu^{\beta-1} - 1$$

Navarro-Frenk-White profile (NFW)

$$\rho_{NFW} = \frac{\rho_s}{(r/r_s)(1 + r/r_s)^2}$$

Singular Isothermal Sphere profile (SIS)

$$\rho_{SIS} = \frac{\sigma_v^2}{2\pi G r^2}$$

Mass density profiles

CCF between lenses-background

$$w_x(\theta; z_l, z_b) = \mu^{\beta-1} - 1$$

Navarro-Frenk-White profile (NFW)

$$\rho_{NFW} = \frac{\rho_s}{(r/r_s)(1+r/r_s)^2}$$

Singular Isothermal Sphere profile (SIS)

$$\rho_{SIS} = \frac{\sigma_v^2}{2\pi G r^2}$$

The Sérsic profile

$$\Sigma_{Sersic} = \Sigma_e \cdot exp\left(-b_n\left(\left(\frac{\theta}{\theta_e}\right)^{1/n} - 1\right)\right)$$

Mass density profiles

CCF between lenses-background

$$w_x(\theta; z_l, z_b) = \mu^{\beta-1} - 1$$

Navarro-Frenk-White profile (NFW)

$$\rho_{NFW} = \frac{\rho_s}{(r/r_s)(1 + r/r_s)^2}$$

Singular Isothermal Sphere profile (SIS)

$$\rho_{SIS} = \frac{\sigma_v^2}{2\pi G r^2}$$

The Sérsic profile

$$\Sigma_{Sersic} = \Sigma_e \cdot exp\left(-b_n\left(\left(\frac{\theta}{\theta_e}\right)^{1/n} - 1\right)\right)$$

Burkert profile

$$\rho_{Burkert} = \frac{\rho_0 r_c^3}{(r + r_c)(r^2 + r_c^2)}$$

1. Introduction
2. Data and Methodology
3. Results
4. Conclusions

H-ATLAS vs WISE

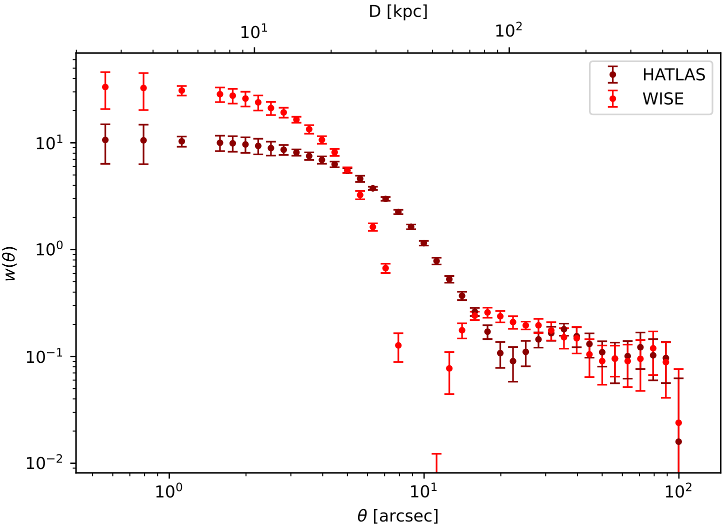

H-ATLAS vs WISE

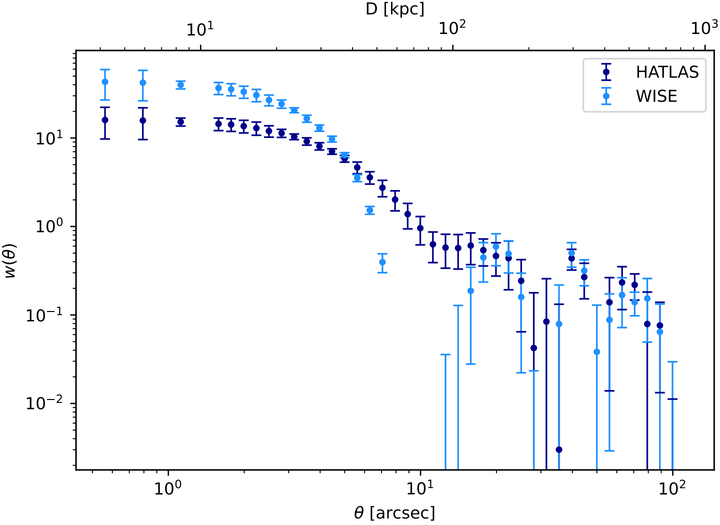

H-ATLAS vs WISE

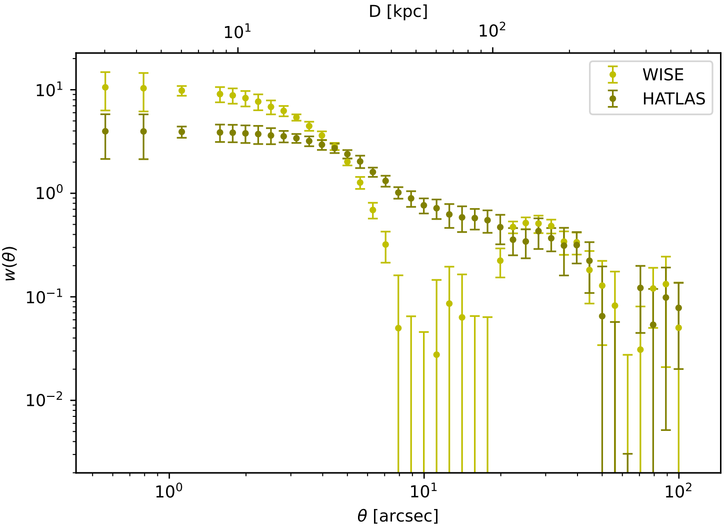

H-ATLAS vs WISE

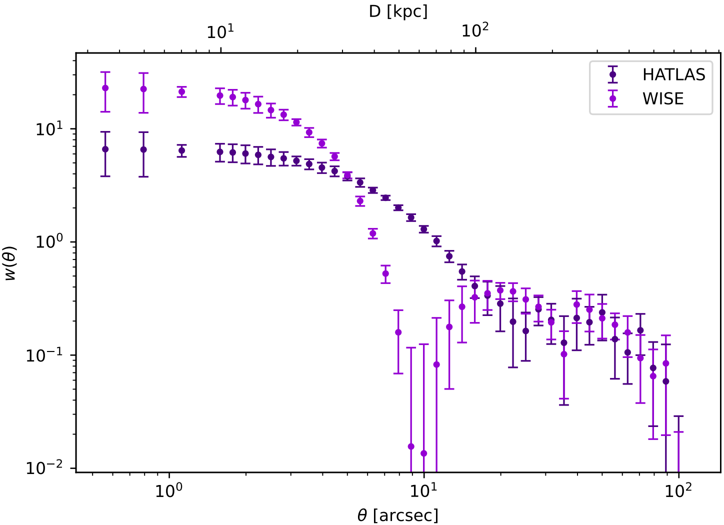

Low-resolution vs High-resolution

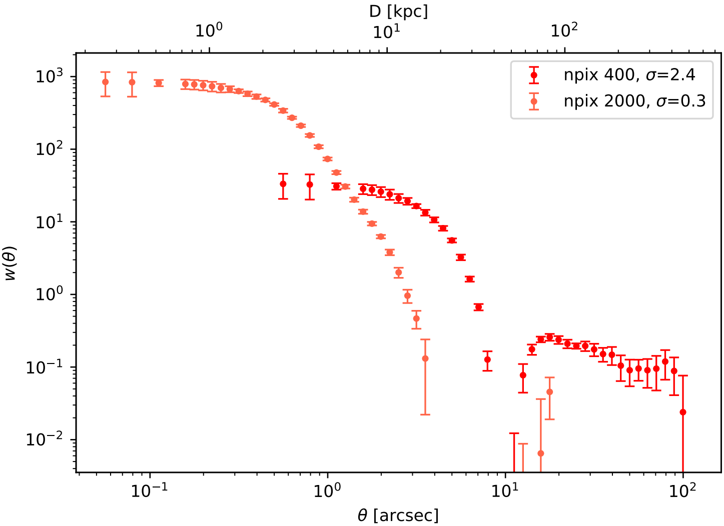

Low-resolution vs High-resolution

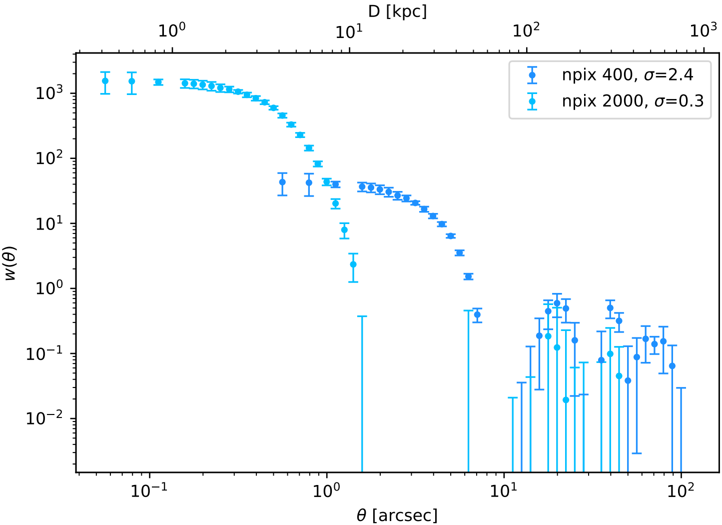

Low-resolution vs High-resolution

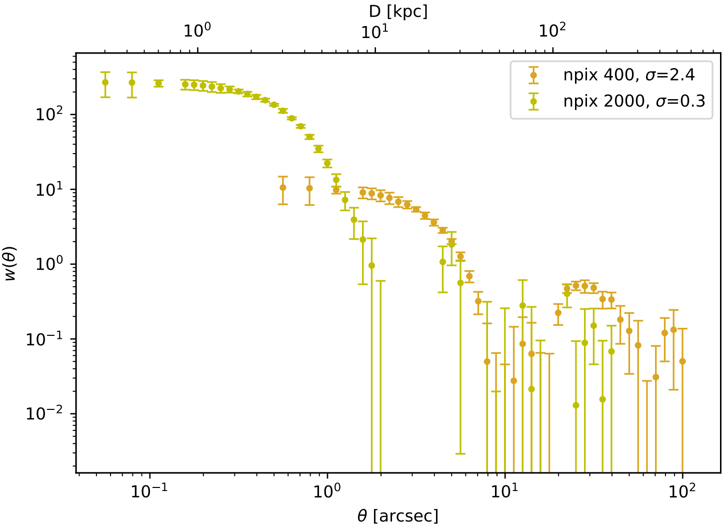

Low-resolution vs High-resolution

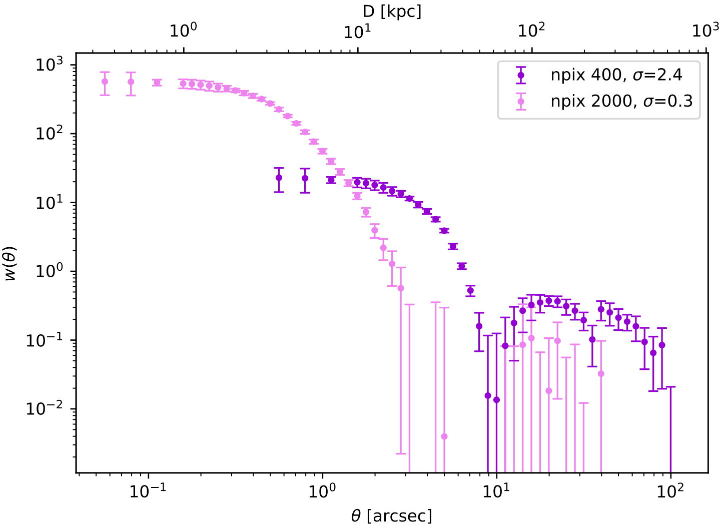

Galaxies case

npix=400 σ=2.4 arcsec

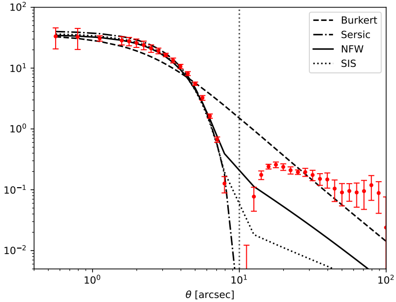

- $M_{SIS} = 2.51 \cdot 10^{11} M_\odot$

- $M_{NFW} = 3.16 \cdot 10^{12} M_\odot$
- $C = 8.5$

- $\Sigma_{e(Sersic)} = 3.98 \cdot 10^{11} M_\odot / Mpc^2$
- $\theta_e = 1.6$ arsec
- n=4

- $\rho_0 = 2.1 \cdot 10^{-2} M_\odot / pc^3$
- $r_c = 40 kpc$

Galaxies case

npix=2000 σ=0.3 arcsec

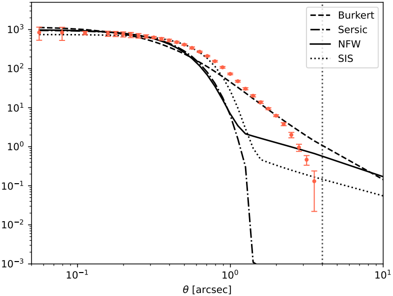

- $M_{SIS} = 1.00 \cdot 10^{12} M_\odot$

- $M_{NFW} = 3.98 \cdot 10^{12} M_\odot$
- $C = 8.00$

- $\Sigma_{e(Sersic)} = 1.00 \cdot 10^{12} M_\odot / Mpc^2$
- $\theta_e = 1.0$ arsec
- n=4

- $\rho_0 = 11.5 \cdot 10^{-2} M_\odot / pc^3$
- $r_c = 10 kpc$

QSOs case

npix=400 σ=2.4 arcsec

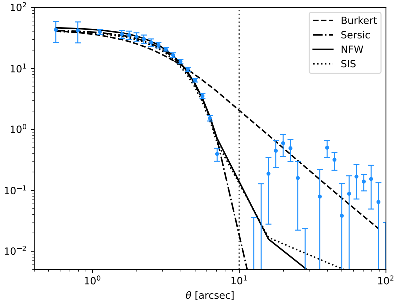

- $M_{SIS} = 5.01 \cdot 10^{11} M_{\odot}$
- $M_{NFW} = 1.26 \cdot 10^{12} M_{\odot}$
- $C = 10.0$
- $\Sigma_{e(Sersic)} = 7.94 \cdot 10^{11} M_{\odot}/Mpc^2$
- $\theta_e = 5.2$ arsec
- n=4
- $\rho_0 = 0.8 \cdot 10^{-2} M_{\odot}/pc^3$
- $r_c = 100 kpc$

QSOs case

npix=2000 σ=0.3 arcsec

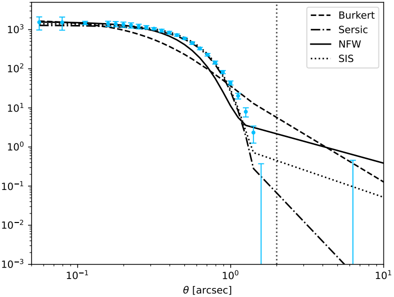

- $M_{SIS} = 1.00 \cdot 10^{12} M_{\odot}$
- $M_{NFW} = 2.51 \cdot 10^{12} M_{\odot}$
- $C = 8.9$
- $\Sigma_{e(Sersic)} = 1.00 \cdot 10^{12} M_{\odot}/Mpc^2$
- $\theta_e = 2.1$ arsec
- n=4
- $\rho_0 = 5.5 \cdot 10^{-2} M_{\odot}/pc^3$
- $r_c = 20kpc$

Clusters Wen catalogue case

npix=400 σ=2.4 arcsec

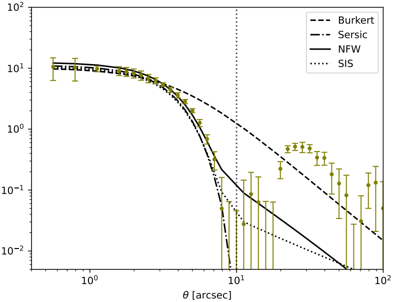

- $M_{SIS} = 5.01 \cdot 10^{11} M_\odot$
- $M_{NFW} = 2.51 \cdot 10^{12} M_\odot$
- $C = 8.5$
- $\Sigma_{e(Sersic)} = 1.00 \cdot 10^{12} M_\odot / Mpc^2$
- $\theta_e = 3.3$ arsec
- n=4
- $\rho_0 = 1.0 \cdot 10^{-2} M_\odot / pc^3$
- $r_c = 60 kpc$

Clusters Wen catalogue case

npix=2000 σ=0.3 arcsec

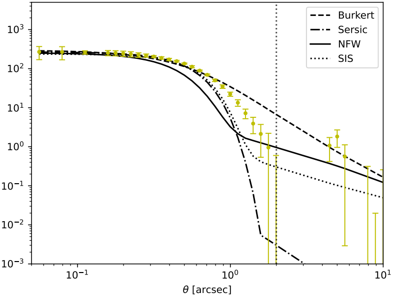

- $M_{SIS} = 1.00 \cdot 10^{12} M_{\odot}$
- $M_{NFW} = 3.16 \cdot 10^{12} M_{\odot}$
- $C = 8.0$
- $\Sigma_{e(Sersic)} = 6.30 \cdot 10^{12} M_{\odot}/Mpc^2$
- $\theta_e = 1.0$ arsec
- n=4
- $\rho_0 = 6.7 \cdot 10^{-2} M_{\odot}/pc^3$
- $r_c = 15 kpc$

Clusters Zou catalogue case

npix=400 σ=2.4 arcsec

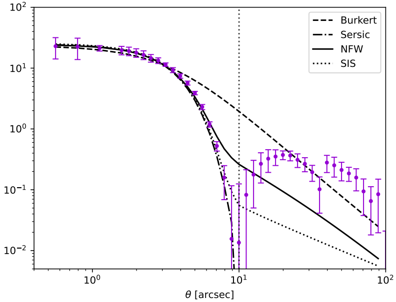

- $M_{SIS} = 1.00 \cdot 10^{12} M_\odot$
- $M_{NFW} = 7.94 \cdot 10^{12} M_\odot$
- $C = 5.4$
- $\Sigma_{e(Sersic)} = 7.94 \cdot 10^{11} M_\odot / Mpc^2$
- $\theta_e = 3.3$ arsec
- n=4
- $\rho_0 = 0.8 \cdot 10^{-2} M_\odot / pc^3$
- $r_c = 80 kpc$

Clusters Zou catalogue case

npix=2000 σ=0.3 arcsec

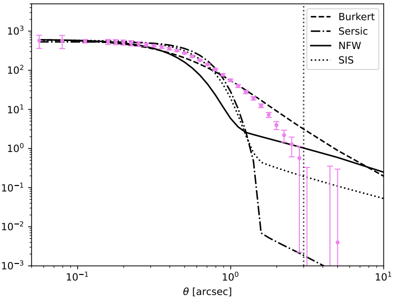

- $M_{SIS} = 1.00 \cdot 10^{12} M_\odot$
- $M_{NFW} = 7.94 \cdot 10^{12} M_\odot$
- $C = 5.4$
- $\Sigma_{e(Sersic)} = 7.94 \cdot 10^{11} M_\odot / Mpc^2$
- $\theta_e = 3.3$ arsec
- n=4
- $\rho_0 = 5.0 \cdot 10^{-2} M_\odot / pc^3$
- $r_c = 20 kpc$

Analysis of the lack of signal

Galaxy cluster satellite positions

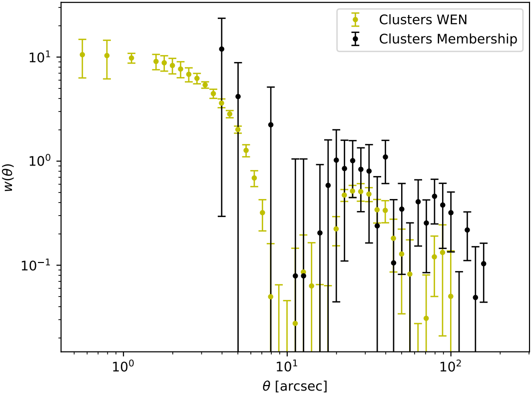

28 Clusters from:

- Berkeley 67, King 2, NGC 2420, NGC 2477, NGC 2682, NGC 6940 (Jadhav et al. 2021)
- IC 2391 (Platais et al. 2007)
- NGC 3532 (Fritzewski et al. 2019)
- NGC 6366 (Sariya & Yadav 2015)
- NGC 6530 (Zhao et al. 2006)
- BPMG, Cha I, IC 2395, IC 348, IC 4665, LCC, NGC 1333, NGC 1960, NGC 2232, NGC 2244, NGC 2362, NGC 2547, Pleiades, THA, Taurus, UCL, Upper Sco (Meng et al. 2017)
- NGC 2548 (Wu et al. 2002)

Analysis of the lack of signal

Galaxy cluster satellite positions

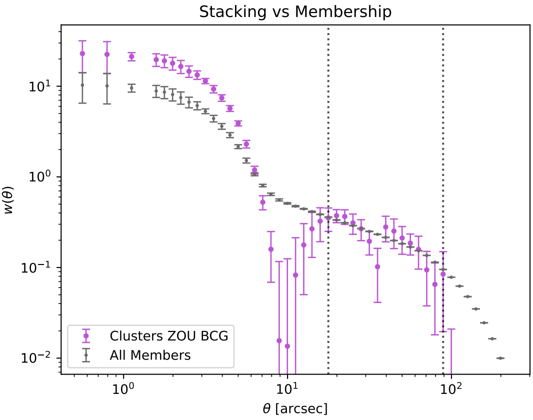

540.433 Clusters from Zou et al. 2021

Analysis of the lack of signal.

Magnification bias simulation

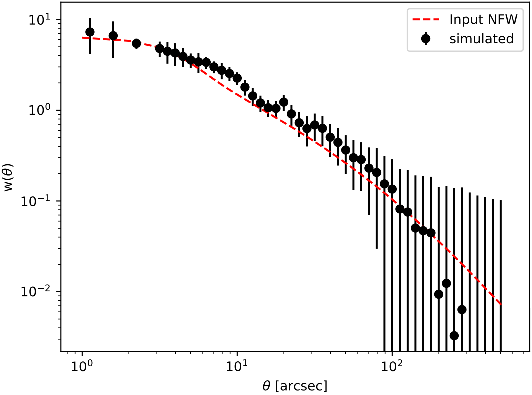

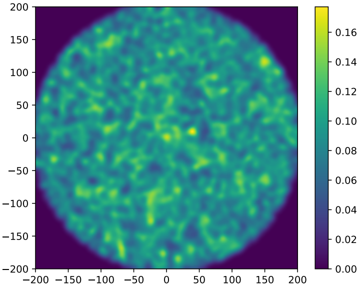

Magnification due to lensing

Analysis of the lack of signal.

Magnification bias simulation

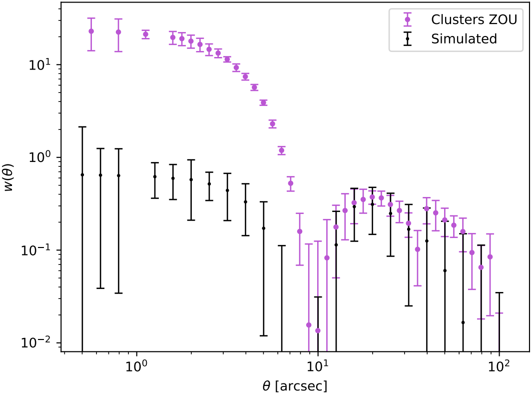

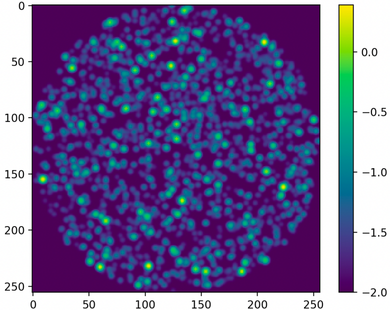

Strong Lensing effects using ray-tracing methodology.

doi: 10.1051/0004-6361/202347426

Analysis of the lack of signal.

Magnification bias simulation

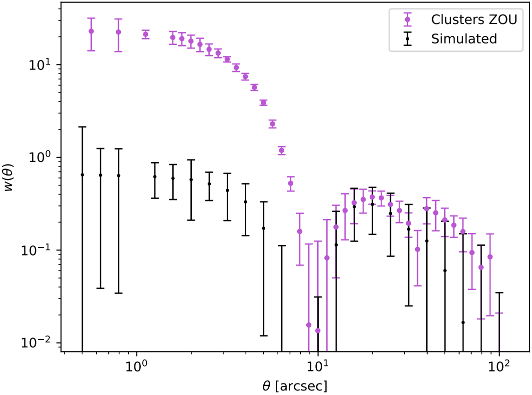

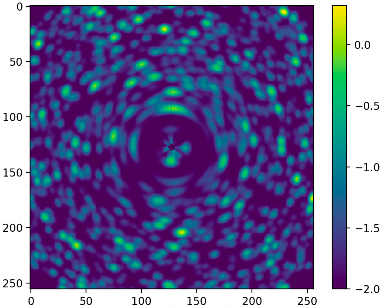

Strong Lensing effects using ray-tracing methodology.

Conclusions

- WISE positions reveal two distinct regimes separated by a region with a lack of signal.
- QSOs producing the strongest signal and WEN clusters exhibiting weaker signals.
- Low-resolution data show "point-like" central mass distribution for all lens types, fitting well with most profiles except Burkert.
- Higher resolution provides more detailed information, allowing clearer distinctions between lens types.
- Central excess shifts to smaller angular separations with higher values $\rightarrow$ increase in the signal void region around 3-5 arcsec for all cases.
- Further detailed analysis of cluster members reveals that the effect is not due to a lack of mass.
- A new simulator incorporating strong lensing effects suggests that these could explain the observed signal void.

Conclusions

- WISE positions reveal two distinct regimes separated by a region with a lack of signal.
- QSOs producing the strongest signal and WEN clusters exhibiting weaker signals.
- Low-resolution data show "point-like" central mass distribution for all lens types, fitting well with most profiles except Burkert.
- Higher resolution provides more detailed information, allowing clearer distinctions between lens types.
- Central excess shifts to smaller angular separations with higher values $\rightarrow$ increase in the signal void region around 3-5 arcsec for all cases.
- Further detailed analysis of cluster members reveals that the effect is not due to a lack of mass.
- A new simulator incorporating strong lensing effects suggests that these could explain the observed signal void.

Conclusions

- WISE positions reveal two distinct regimes separated by a region with a lack of signal.
- QSOs producing the strongest signal and WEN clusters exhibiting weaker signals.
- Low-resolution data show "point-like" central mass distribution for all lens types, fitting well with most profiles except Burkert.
- Higher resolution provides more detailed information, allowing clearer distinctions between lens types.
- Central excess shifts to smaller angular separations with higher values $\rightarrow$ increase in the signal void region around 3-5 arcsec for all cases.
- Further detailed analysis of cluster members reveals that the effect is not due to a lack of mass.
- A new simulator incorporating strong lensing effects suggests that these could explain the observed signal void.

Conclusions

- WISE positions reveal two distinct regimes separated by a region with a lack of signal.
- QSOs producing the strongest signal and WEN clusters exhibiting weaker signals.
- Low-resolution data show "point-like" central mass distribution for all lens types, fitting well with most profiles except Burkert.
- Higher resolution provides more detailed information, allowing clearer distinctions between lens types.
- Central excess shifts to smaller angular separations with higher values → increase in the signal void region around 3-5 arcsec for all cases.
- Further detailed analysis of cluster members reveals that the effect is not due to a lack of mass.
- A new simulator incorporating strong lensing effects suggests that these could explain the observed signal void.

Conclusions

- WISE positions reveal two distinct regimes separated by a region with a lack of signal.
- QSOs producing the strongest signal and WEN clusters exhibiting weaker signals.
- Low-resolution data show "point-like" central mass distribution for all lens types, fitting well with most profiles except Burkert.
- Higher resolution provides more detailed information, allowing clearer distinctions between lens types.
- Central excess shifts to smaller angular separations with higher values $\rightarrow$ increase in the signal void region around 3-5 arcsec for all cases.
- Further detailed analysis of cluster members reveals that the effect is not due to a lack of mass.
- A new simulator incorporating strong lensing effects suggests that these could explain the observed signal void.

Conclusions

- WISE positions reveal two distinct regimes separated by a region with a lack of signal.
- QSOs producing the strongest signal and WEN clusters exhibiting weaker signals.
- Low-resolution data show "point-like" central mass distribution for all lens types, fitting well with most profiles except Burkert.
- Higher resolution provides more detailed information, allowing clearer distinctions between lens types.
- Central excess shifts to smaller angular separations with higher values $\rightarrow$ increase in the signal void region around 3-5 arcsec for all cases.
- Further detailed analysis of cluster members reveals that the effect is not due to a lack of mass.
- A new simulator incorporating strong lensing effects suggests that these could explain the observed signal void.

Conclusions

- WISE positions reveal two distinct regimes separated by a region with a lack of signal.
- QSOs producing the strongest signal and WEN clusters exhibiting weaker signals.
- Low-resolution data show "point-like" central mass distribution for all lens types, fitting well with most profiles except Burkert.
- Higher resolution provides more detailed information, allowing clearer distinctions between lens types.
- Central excess shifts to smaller angular separations with higher values $\rightarrow$ increase in the signal void region around 3-5 arcsec for all cases.
- Further detailed analysis of cluster members reveals that the effect is not due to a lack of mass.
- A new simulator incorporating strong lensing effects suggests that these could explain the observed signal void.